

# Spectral Response of UV Photodetectors for Barium Fluoride Crystal Readout

Liyuan Zhang, *Member, IEEE*, Chen Hu, *Member, IEEE*, James Oyang, Bertrand Echenard, David Hitlin, Xuebin Qiao, Jason Trevor, and Ren-Yuan Zhu<sup>IP</sup>, *Senior Member, IEEE*

**Abstract**—Because of its fast scintillation peaked at 220 nm with a decay time of less than 0.6 ns, barium fluoride crystals have attracted broad interest in the community pursuing ultrafast detectors for future high energy physics (HEP) experiments and GHz hard X-ray imaging for future X-ray free-electron laser (XFEL) facilities. A crucial issue for its application is the spectral response of photodetectors down to vacuum ultraviolet (VUV). In this article, we compare quantum efficiency (QE) and photon detection efficiency (PDE) spectra measured for several ultraviolet (UV) photodetectors down to 200 nm. Their figures of merit on the detection efficiency for the fast component and the suppression of the slow component are also discussed.

**Index Terms**—Barium fluoride, photomultiplier, photon detection efficiency (PDE), quantum efficiency (QE), silicon photomultiplier (SiPM), ultrafast scintillator.

## I. INTRODUCTION

**B**ECAUSE of its fast cross-luminescence [1]–[7] peaked at 220 nm with a decay time of less than 0.6 ns [8]–[15], barium fluoride ( $\text{BaF}_2$ ) crystals have attracted broad interest in the community pursuing ultrafast calorimetry for future high energy and nuclear physics experiments [14], [19] and GHz hard X-ray imaging for future X-ray free-electron laser (XFEL) facilities [9], [13]. One crucial issue preventing  $\text{BaF}_2$  application is its slow scintillation component peaked at 300 nm due to self-trapped excitons with a decay time of 600 ns and an intensity of more than five times of the fast component, which causes pileup and readout noise in a high-rate environment.

A  $\text{BaF}_2$  crystal calorimeter was baselined for the Mu2e experiment [14] and was replaced by an undoped CsI crystal calorimeter mainly due to this slow component [15]. It is also well known that undoped CsI survives the Mu2e radiation environment where an ionization dose is up to a few tens krad but not a few hundred krad expected by Mu2e-II.  $\text{BaF}_2$ , on the other hand, is found more radiation hard against an ionization dose up to 200 Mrad [16], a proton fluence up to  $1 \times 10^{15}$  p/cm<sup>2</sup> [17], and a neutron fluence up to  $9 \times 10^{15}$  n<sub>eq</sub>/cm<sup>2</sup> [18]. To cope with the unprecedented event rate, a  $\text{BaF}_2$  crystal-based ultrafast calorimeter is proposed for the

Manuscript received December 12, 2021; accepted February 5, 2022. Date of publication February 7, 2022; date of current version April 19, 2022. This work was supported by the U.S. Department of Energy, Office of High Energy Physics Program, under Award DE-SC0011925.

The authors are with the HEP, California Institute of Technology, Pasadena, CA 91125 USA (e-mail: zhu@caltech.edu).

Color versions of one or more figures in this article are available at <https://doi.org/10.1109/TNS.2022.3149840>.

Digital Object Identifier 10.1109/TNS.2022.3149840

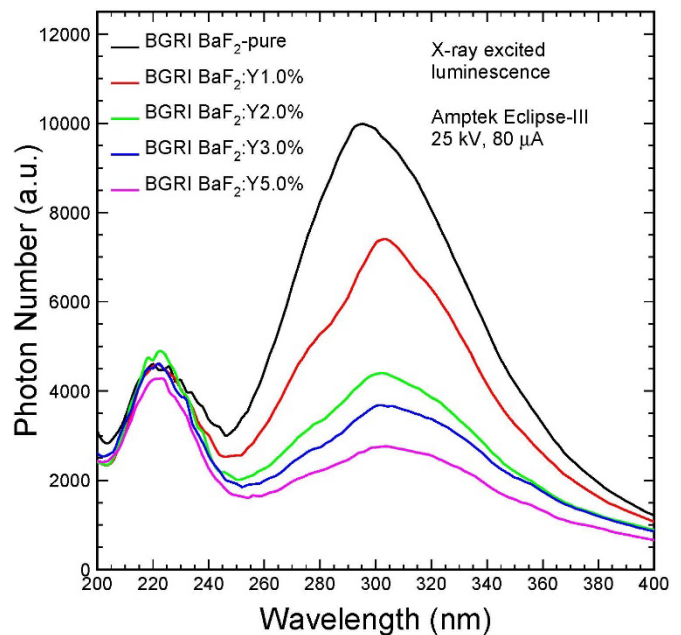


Fig. 1. X-ray excited emission spectra measured for  $\text{BaF}_2$  crystal samples with different yttrium doping levels [31].

Mu2e-II experiment [19]. One crucial issue is the pile-up and readout noise caused by the slow component. Research and development have been going on in two directions to address this issue. One is selective rare-earth or transition metal doping in  $\text{BaF}_2$  crystals [20]–[32]. The other is to use solar-blind photodetectors sensitive only to the fast component at 220 nm but not the slow component at 300 nm [27], [33]–[35].

Progress has been achieved in both directions. Fig. 1 shows X-ray excited emission spectra measured for  $\text{BaF}_2$  crystal samples with different yttrium doping levels, showing consistent fast scintillation component, and significantly suppressed slow component with increased yttrium doping level [31]. The recent investigation also shows that solar-blind ultraviolet (UV) photodetectors are needed to further suppress the slow component and reduce radiation-induced readout noise to a level of less than 1 MeV for  $\text{BaF}_2$  crystals of Mu2e size [36]. In this article, we report quantum efficiency (QE) and photon detection efficiency (PDE) spectra measured for several UV/vacuum UV (VUV) photodetectors down to 200 nm. Their figure of merit on the detection efficiency for the fast component and the slow component suppression is also discussed.

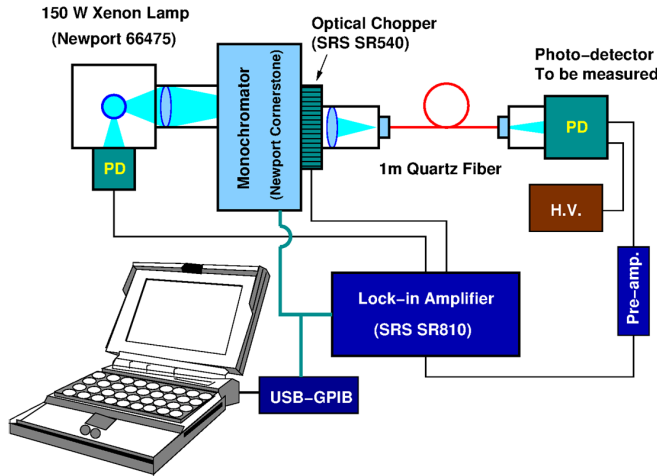


Fig. 2. Setup used to measure QE and PDE as a function of wavelength.

## II. EXPERIMENTAL SETUP AND PHOTODETECTORS

Fig. 2 shows a test bench used to measure QE and PDE as a function of wavelength. A UV extended 150-W Xenon lamp was used as the light source. The fluctuation of the light source intensity was monitored by a photodiode mounted on the lamphouse and corrected through a lock-in amplifier (Stanford Research Systems SR810). A narrow wavelength band was selected by a monochromator, chopped by an optical chopper, and coupled to a 1-mm quartz fiber with  $NA = 0.22$ . The light pulses from the fiber were centered to a  $\Phi 5$ -mm area of the photodetector to be measured. The response of the photodetector was scanned from 200 to 800 nm and was read out through a low noise pre-amplifier (Newport 70710) and the lock-in amplifier.

For photodetectors with a unit gain, their  $QE(\lambda)$  is obtained by normalizing its response  $R(\lambda)$  to the response of a NIST traceable reference Si-PD (Newport 71650)  $R_{PD}(\lambda)$  scanned under the same settings, as shown in the following equation:

$$QE(\lambda) = \frac{R(\lambda)}{R_{PD}(\lambda)} QE_{PD}(\lambda). \quad (1)$$

The QE of four Hamamatsu R2059 PMTs and a Photek solar-blind photocathode diode was measured, where a homemade socket connected all dynodes to set their gain to one.

For photodetectors with gain, such as SiPM, the normalized response  $R(\lambda)$  is a product of the PDE and the gain, so it is a relative PDE. The calibration of SiPM PDE was carried out by using a 465-nm blue LED. Fig. 3 shows a scope trace of SiPM response (red) to LED pulses of 10-ns FWHM. The charge of the SiPM output pulses was integrated by a LeCroy 3001 qvt in 800-ns gate (blue dots) and digitized for a pulse height spectrum.

Figs. 4 and 5 show the pulse height spectra measured by two FBK research and development SiPMs, sn612-A1 and sn615-A1, integrated with UV filters I and II, respectively, with breakdown voltages of 25.0 and 31.5 V. Also shown in the figures are the numerical values of the position and widths of photopeak and pedestal.

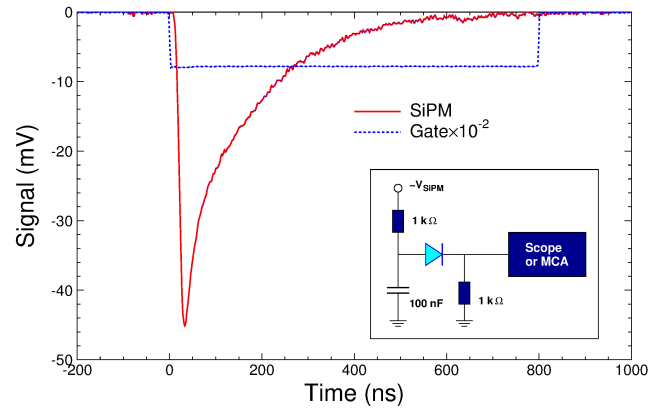


Fig. 3. SiPM output pulse (red) to 10-ns pulse from a 465-nm blue LED is shown in an 800-ns gate (blue dots) for pulse height spectra.

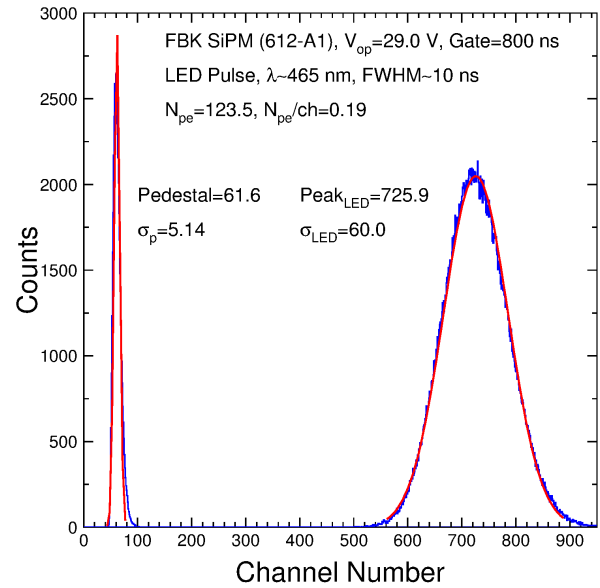


Fig. 4. Pulse height spectrum of an FBK SiPM (612-A1,  $V_{br} = 25.0$  V) with UV filter I measured by using a 10-ns light pulse from a 465-nm LED.

The photoelectron (p.e.) number of the photopeak was calculated according to the following equation:

$$N_{p.e.} = \frac{(P_{LED} - P_P)^2}{\sigma_{LED}^2 - \sigma_P^2} \quad (2)$$

where  $P_{LED}$  and  $\sigma_{LED}$  are the LED photopeak and width, and  $P_P$  and  $\sigma_P$  are the pedestal peak and width. The photoelectron number was determined as 123.5 and 152.3 for these two FBK SiPMs, respectively.

The input photon number from LED pulses was determined by measuring the dc current by a reference Si-PD with known QE according to the following equation:

$$N_{ph} = \frac{I_{PD}/S}{h\nu_{LED} \times f_{LED}} \quad (3)$$

where  $I_{PD}$  and  $S$  are the photocurrent and sensitivity of the reference Si-PD, and  $h\nu_{LED}$  and  $f_{LED}$  are the LED photon energy and the pulse rate.

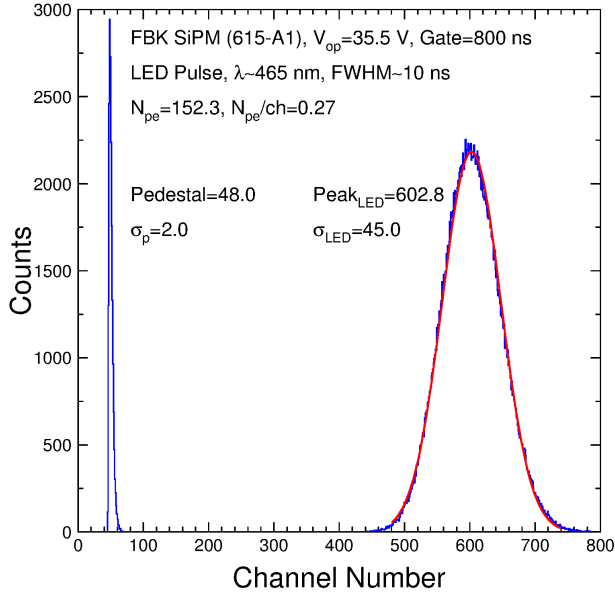


Fig. 5. Pulse height spectrum of FBK SiPM (615-A1,  $V_{br} = 31.5$  V) with UV filter II measured by using a 10-ns light pulse from a 465-nm LED.

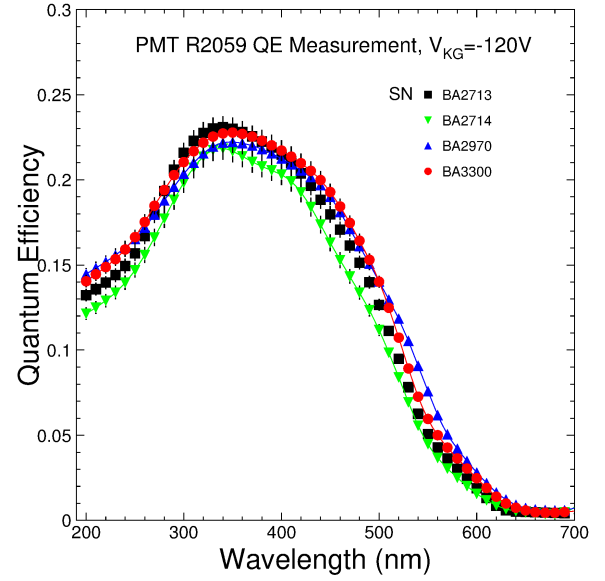


Fig. 7. Measured QE (200–700 nm) of four Hamamatsu R2059 PMTs.

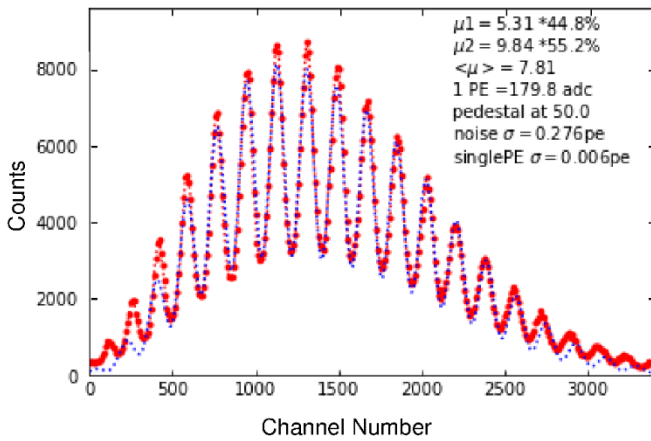


Fig. 6. Individual photoelectron peaks observed by an FBK SiPM responding to attenuated LED pulses.

The PDE value at 465 nm was determined as the following equation:

$$\text{PDE}(465 \text{ nm}) = \frac{N_{p.e.}}{N_{ph}}. \quad (4)$$

$\sigma_{LED}$ , obtained from the Gaussian fitting, however, is affected by the excess noise factor (ENF) of the photodetector. A cross-check was carried out by measuring the response of a Hamamatsu R2059 PMT with a gain provided by a normal base socket. The resultant ENF was found to be about 1.1, which is consistent with the Hamamatsu technical note. The ENF values for SiPMs were also measured. Fig. 6 shows that individual photon electron peaks can be clearly resolved in SiPM response to attenuated LED pulses by using an amplifier (Ortec VT120) and digitizer (CAEN V1720). The ENF values were determined as the ratio between the photoelectron numbers from this single p.e. calibration to that from (2).

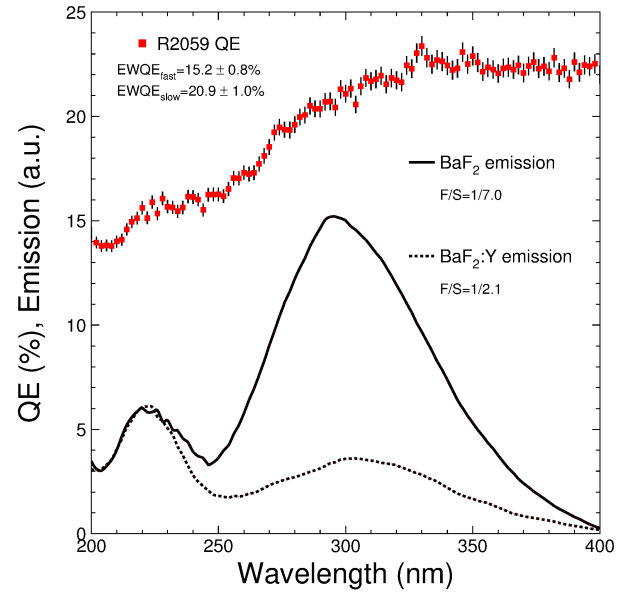


Fig. 8. Measured QE (200–400 nm) of a Hamamatsu R2059 PMT and the X-ray excited emission spectra of  $\text{BaF}_2$  and  $\text{BaF}_2:\text{Y}$ .

After the ENF correction shown in (5), the PDE values at 465 nm are 6.3% and 35.1% for two FBK SiPMs with Type I and II filters, respectively,

$$\text{PDE}(465 \text{ nm}) = \frac{N_{p.e.}}{N_{ph}} \times \text{ENF}. \quad (5)$$

The PDE of four Hamamatsu MPPCs (or SiPMs) and several FBK research and development SiPMs with integrated UV filter was obtained by using the relative PDE  $R(\lambda)$  from 200 to 600 nm and the 465-nm calibration.

### III. RESULTS AND DISCUSSION

Fig. 7 shows consistent QE spectra between 200 and 700 nm for four Hamamatsu R2059 PMTs.

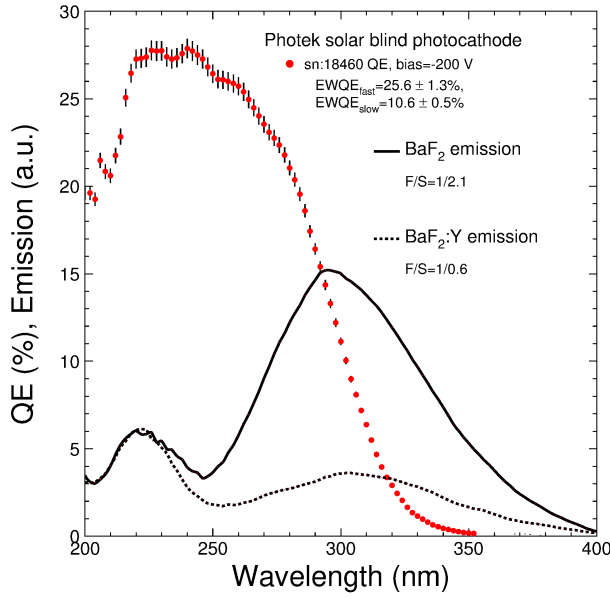


Fig. 9. Measured QE (200–400 nm) of Photek solar-blind photocathode and the X-ray excited emission spectra of BaF<sub>2</sub> and BaF<sub>2</sub>:Y.

Fig. 8 shows the measured QE spectrum (red dots with error bars) between 200 and 400 nm for an R2059 PMT and the X-ray excited emission spectra of BaF<sub>2</sub> (black solid lines) and BaF<sub>2</sub>:Y with suppressed slow emission (black dashed lines). Also shown in the figure are the numerical values of the emission weighted QE (EWQE) defined as

$$\text{EWQE}_{\text{fast/slow}} = \frac{\int_{\lambda_1}^{\lambda_2} \text{Em}(\lambda) \text{QE}(\lambda) d\lambda}{\int_{\lambda_1}^{\lambda_2} \text{Em}(\lambda) d\lambda} \quad (6)$$

where  $\text{Em}(\lambda)$  is the X-ray excited emission spectrum of BaF<sub>2</sub> or BaF<sub>2</sub>:Y;  $\lambda_1 = 200$  and  $250$  nm and  $\lambda_2 = 250$  and  $400$  nm, respectively, for the fast and slow lights. The  $\text{EWQE}_{\text{fast}}$  and  $\text{EWQE}_{\text{slow}}$  values are  $15.2\%$  and  $20.9\%$ , respectively, for the fast and slow lights. Since the emission spectra of BaF<sub>2</sub> and BaF<sub>2</sub>:Y have a similar line shape (with different intensity for the slow light), the corresponding emission weighted QE values are the same for both BaF<sub>2</sub> and BaF<sub>2</sub>:Y. Also shown in the figure is the ratio between the fast and slow scintillation light ( $F/S$ ) for BaF<sub>2</sub> and BaF<sub>2</sub>:Y, which are defined as

$$\frac{F}{S} = \frac{\int_{200 \text{ nm}}^{250 \text{ nm}} \text{Em}(\lambda) \text{QE}(\lambda) d\lambda}{\int_{250 \text{ nm}}^{400 \text{ nm}} \text{Em}(\lambda) \text{QE}(\lambda) d\lambda}. \quad (7)$$

The  $\text{EWQE}_{\text{fast}}$  and the  $F/S$  ratio are considered as the figures of merit representing the photodetector's ability for fast detection and slow suppression, respectively. While the  $\text{EWQE}_{\text{fast}}$  values are  $0.15$  for both BaF<sub>2</sub> and BaF<sub>2</sub>:Y, their  $F/S$  ratio values are  $1/7$  and  $1/2.1$ , respectively, for the Hamamatsu R2059, indicating a factor of  $3.5$  improvements in the slow suppression provided by BaF<sub>2</sub>:Y.

Fig. 9 shows the measured QE between 200 and 400 nm for the Photek solar-blind photocathode. The EWQEs for fast and slow components are  $25.6\%$  and  $10.6\%$ , respectively, showing a high detection efficiency and a clear selective readout for the fast component. While the  $\text{EWQE}_{\text{fast}}$  values

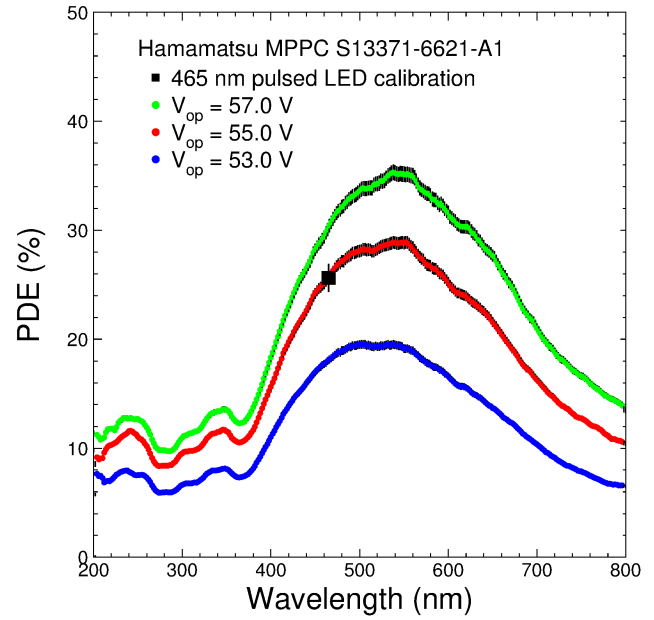


Fig. 10. Measured PDE (200–800 nm) of the Hamamatsu VUV3 MPPC (S13371-6621-A1,  $V_{\text{br}} = 51.0$  V) at operation voltage of 53, 55, and 57 V.

are  $0.26$  for both BaF<sub>2</sub> and BaF<sub>2</sub>:Y, the  $F/S$  values are  $1/0.6$  and  $1/2.1$ , indicating, once again, a factor of  $3.5$  better slow suppression for BaF<sub>2</sub>:Y. Compared to the bi-alkali cathode of Hamamatsu 2059 shown in Fig. 10, the Photek solar-blind cathode shows a factor of  $1.5$  better efficiencies for fast detection and another factor of  $3.5$  better for slow suppression.

Fig. 10 shows PDE for the Hamamatsu VUV3 MPPC S13371-6621-A1 ( $V_{\text{br}} = 51.0$  V) between 200 and 800 nm with three operation voltages of 53 (blue), 55 (red), and 57 (green) V. Also shown in the figure is the 465-nm blue LED calibration at the nominal operating voltage 55 V.

Fig. 11 shows PDE between 200 and 400 nm for the Hamamatsu VUV3 MPPC S13371-6621-A1 at the nominal operating voltage of 55.0 V. Its low  $\text{EWQE}_{\text{fast}}$  values of  $0.10$  indicate a low detection efficiency for the fast component. Its  $F/S$  values are  $1/4.8$  and  $1/1.5$ , respectively, for BaF<sub>2</sub> and BaF<sub>2</sub>:Y crystals respectively, indicating a factor of  $3.2$  better slow suppression for BaF<sub>2</sub>:Y. Compared to PMTs, its  $F/S$  ratio is better than the bi-alkali cathode (R2059) but worse than Photek solar-blind cathode.

Fig. 12 shows measured PDE spectra between 200 and 600 nm for the FBK SiPM integrated with the type I UV bandpass filter (sn:612-A1,  $V_{\text{br}} = 25.0$  V) at operation voltages of 27.5, 29.0, and 30.5 V. Also shown in the figure is the 465-nm blue LED calibration done at the nominal operating voltage of 29 V.

Fig. 13 shows its PDE (200–400 nm) at 30.5 V and the X-ray excited emission spectra of BaF<sub>2</sub> and BaF<sub>2</sub>:Y. The emission weighted photon detection efficiencies (EWPDE) are  $17.8\%$  and  $12.7\%$  for the fast and slow components. The figures of merit are  $0.18$  for the fast component detection and  $1/3.6$  and  $1/1.1$  for the  $F/S$  ratio for BaF<sub>2</sub> and BaF<sub>2</sub>:Y, respectively, indicating a promising solution for slow suppression. Research and development will be continued in this direction.

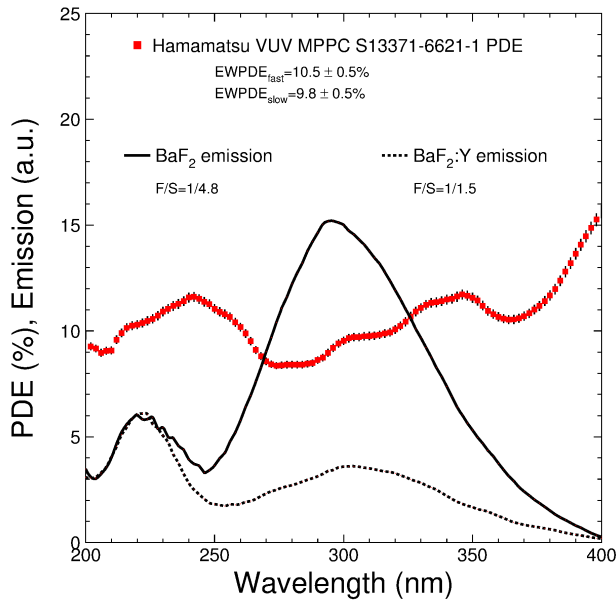


Fig. 11. Measured PDE (200–400 nm) of the Hamamatsu VUV3 MPPC and the X-ray excited emission spectra of BaF<sub>2</sub> and BaF<sub>2</sub>:Y.

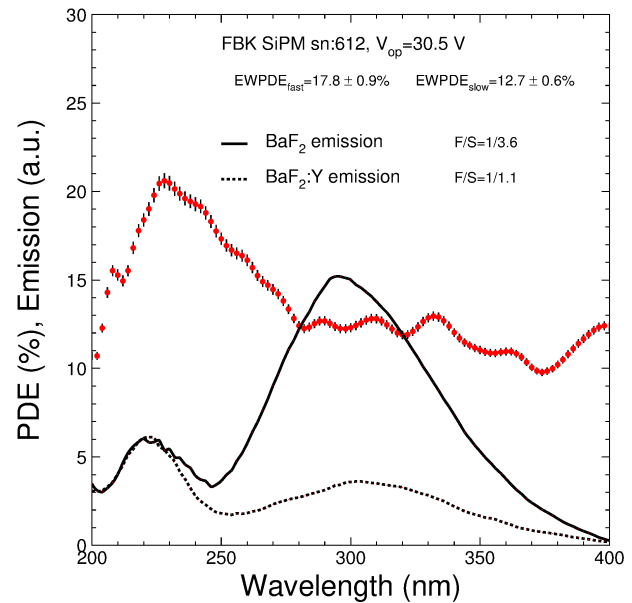


Fig. 13. Measured PDE (200–400 nm) of the FBK SiPM 612-A1 at 30.5 V and the X-ray excited emission spectra of BaF<sub>2</sub> and BaF<sub>2</sub>:Y.

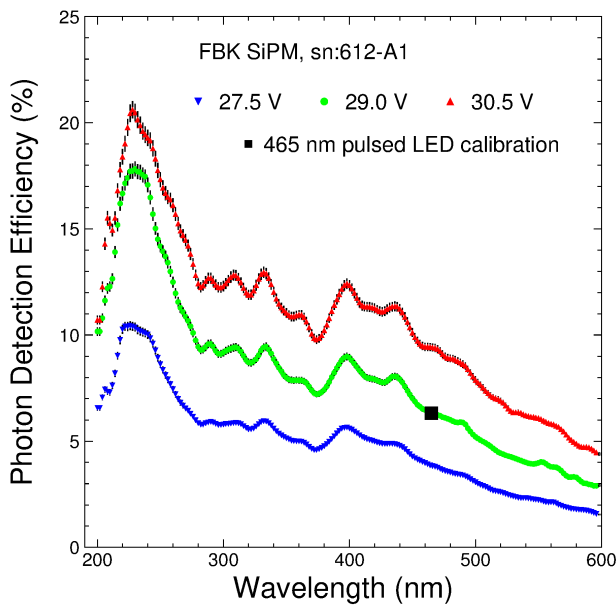


Fig. 12. Measured PDE (200–600 nm) of the FBK SiPM sn:612-A1 with the UV filter I at operation voltages of 27.5, 29.0, and 30.5 V, and  $V_{br} = 25.0$  V.

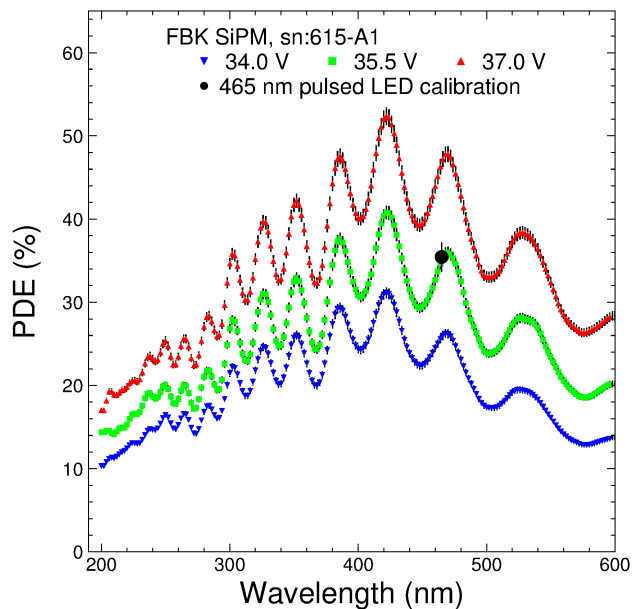


Fig. 14. Measured PDE (200–600 nm) of the FBK SiPM sn:615-A1 with the UV filter II at operation voltages of 34.0, 35.5, and 37.0 V, and  $V_{br} = 31.5$  V.

Fig. 14 shows the measured PDE spectra between 200 and 600 nm for the FBK SiPM integrated with the type II UV filter (sn:615-A1,  $V_{br} = 31.5$  V) at operation voltages of 34.0, 35.5, and 37.0 V. The observed oscillation is consistent with the filter design. Also shown in the figure is the 465-nm blue LED calibration at the nominal operation voltage of 35.5 V.

Fig. 15 shows its PDE (200–400 nm) spectrum at 37 V and the X-ray excited emission spectra of BaF<sub>2</sub> and BaF<sub>2</sub>:Y. The spectral response shows no additional slow suppression with

this type of UV filter. Research and development will not be continued in this direction.

Table I summarized the numerical values for the photodetectors investigated. The first two columns are EWQE/ EWPDE for the fast and slow components. The third and fourth ones are the fast/slow ratio for BaF<sub>2</sub> and BaF<sub>2</sub>:Y crystals, where the slow suppression effect of BaF<sub>2</sub>:Y is shown. While the EWQE/EWPDE is directly related to the light output from a photodetector, the  $F/S$  ratio represents its ability for slow

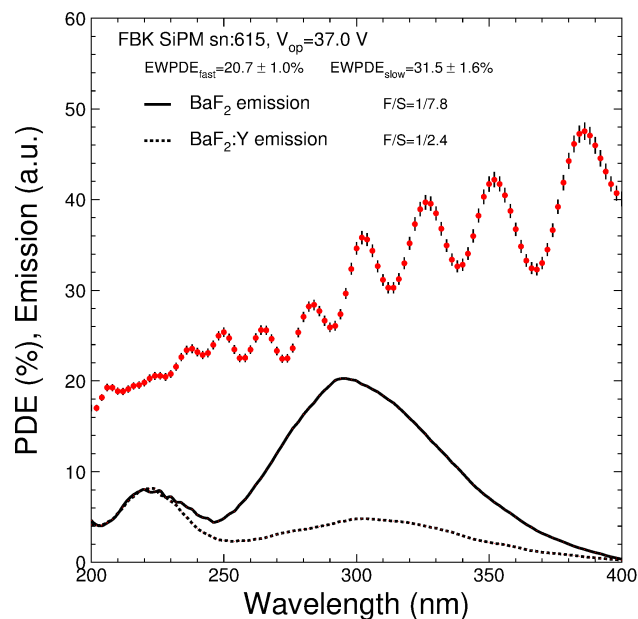


Fig. 15. Measured PDE (200–400 nm) of the FBK SiPM 615-A1 at 37.0 V and the X-ray excited emission spectra of BaF<sub>2</sub> and BaF<sub>2</sub>:Y.

TABLE I

SUMMARY OF THE FIGURES OF MERIT FOR PHOTODETECTORS

Photodetectors	EWQE <sub>fast</sub> (%)	EWQE <sub>slow</sub> (%)	BaF <sub>2</sub> F/S	BaF <sub>2</sub> :Y F/S
Hamamatsu R2059 PMT	15.2	20.9	1/7.0	1/2.1
Hamamatsu MPPC S13371	10.5	9.8	1/4.8	1/1.5
<b>Photek PMT Solar blind</b>	<b>25.6</b>	<b>10.6</b>	<b>1/2.1</b>	<b>1/0.6</b>
<b>FBK SiPM w/UV filter-I</b>	<b>17.8</b>	<b>12.7</b>	<b>1/3.6</b>	<b>1/1.1</b>
FBK SiPM w/UV filter-II	20.7	31.5	1/7.8	1/2.4

suppression. A combination of BaF<sub>2</sub>:Y crystals and selective readout provided by solar-blind photodetectors from either Photek photocathode or FBK SiPM integrated with the type-I UV bandpass filter shows a promising solution.

#### IV. SUMMARY

While yttrium doping in BaF<sub>2</sub> crystals increases the *F/S* ratio by a factor of three, solar-blind photodetectors would further reduce pileup noise for a BaF<sub>2</sub> crystal-based ultrafast calorimeter for future high energy physics (HEP) experiments, such as Mu2e-II. Progress has been made in both solar-blind photocathode and SiPMs with an integrated UV bandpass filter. Research and development are ongoing to further optimize the EWQE/EWPDE<sub>fast</sub> and the *F/S* ratio for BaF<sub>2</sub> crystal readout with photodetectors.

Since a fraction of BaF<sub>2</sub> emission is below 200 nm, we plan to extend the coverage of our QE/PDE test bench to the VUV range down to 175 nm with either vacuum or N<sub>2</sub> purging. Novel VUV photodetectors, such as the Hamamatsu SiPM

investigated in this manuscript and other semiconductor-based VUV photodetectors [37], [38], will also be investigated.

#### ACKNOWLEDGMENT

The authors would like to thank Dr. P. Hink for providing the solar-blind photocathode investigated in this work.

#### REFERENCES

- [1] N. N. Ershov, N. G. Zakharov, and P. A. Rodnyi, "Spectral-kinetic study of the intrinsic-luminescence characteristics of a fluorite-type crystal," *Opt. Spectrosc.*, vol. 53, no. 1, pp. 51–54, Jul. 1982.
- [2] M. Laval *et al.*, "Barium fluoride—Inorganic scintillator for subnanosecond timing," *Nucl. Instrum. Methods Phys. Res.*, vol. 206, nos. 1–2, pp. 169–176, Feb. 1983.
- [3] Y. M. Aleksandrov, V. N. Makhov, P. A. Rodnyi, T. I. Sreyschchikova, and M. N. Yakimenko, "Intrinsic luminescence of BaF<sub>2</sub> at pulsed synchrotron radiation excitation," *Sov. Phys. Solid State*, vol. 26, no. 9, pp. 2865–2867, 1984.
- [4] Y. A. Valbis, Z. A. Rachko, and Y. L. Yansons, "Short-wave UV luminescence of BaF<sub>2</sub> crystals caused by crossover transitions," *Sov. J. Exp. Theor. Phys. Lett.*, vol. 42, no. 4, pp. 140–142, Aug. 1985.
- [5] P. Dorenbos, R. Visser, J. Andriessen, C. W. E. van Eijk, J. Valbis, and N. M. Khaidukov, "Scintillation properties of possible cross-luminescence materials," *Nucl. Tracks Radiat. Meas.*, vol. 21, no. 1, pp. 101–103, Jan. 1993.
- [6] V. N. Makhov, "Vacuum ultraviolet luminescence of wide band-gap solids studied using time-resolved spectroscopy with synchrotron radiation," *Phys. Scripta*, vol. 89, no. 4, Feb. 2014, Art. no. 044010.
- [7] J. Andriessen, P. Dorenbos, and C. W. E. Van Eijk, "Electronic structure and transition probabilities in pure and Ce<sup>3+</sup> doped BaF<sub>2</sub>, an explorative study," *Mol. Phys.*, vol. 74, no. 3, pp. 535–546, Oct. 1991.
- [8] S. E. Dorenzo, M. J. Weber, W. W. Moses, and C. Dujardin, "Measurements of the intrinsic rise times of common inorganic scintillators," *IEEE Trans. Nucl. Sci.*, vol. 47, no. 3, pp. 860–864, Jun. 2000.
- [9] C. Hu *et al.*, "Ultrafast inorganic scintillators for gigahertz hard X-ray imaging," *IEEE Trans. Nucl. Sci.*, vol. 65, no. 8, pp. 2097–2104, Aug. 2018.
- [10] S. Gundacker *et al.*, "Experimental time resolution limits of modern SiPMs and TOF-PET detectors exploring different scintillators and Cherenkov emission," *Phys. Med. Biol.*, vol. 65, no. 2, Jan. 2020, Art. no. 025001.
- [11] R. H. Pots, E. Auffray, and S. Gundacker, "Exploiting cross-luminescence in BaF<sub>2</sub> for ultrafast timing applications using deep-ultraviolet sensitive HPK silicon photomultipliers," *Frontiers Phys.*, vol. 8, p. 482, Oct. 2020.
- [12] R. Novotny, "Performance of the BaF<sub>2</sub>-calorimeter TAPS," *Nucl. Phys. B, Proc. Supplements*, vol. 61, no. 3, pp. 137–142, Feb. 1998.
- [13] R. W. Garnett and M. S. Gulley, "Matter-radiation interactions in extremes," in *Proc. Linear Accel. Conf. (LINA)*, 2010, pp. 485–487.
- [14] G. Pezzullo *et al.*, "Progress status for the Mu2e calorimeter system," *J. Phys., Conf. Ser.*, vol. 587, Feb. 2015, Art. no. 012047.
- [15] N. Atanov *et al.*, "Design and status of the Mu2e crystal calorimeter," *IEEE Trans. Nucl. Sci.*, vol. 65, no. 8, pp. 2073–2080, Aug. 2018.
- [16] F. Yang, L. Zhang, and R.-Y. Zhu, "Gamma-ray induced radiation damage up to 340 Mrad in various scintillation crystals," *IEEE Trans. Nucl. Sci.*, vol. 63, no. 2, pp. 612–619, Apr. 2016.
- [17] C. Hu *et al.*, "Proton-induced radiation damage in BaF<sub>2</sub>, LYSO, and PWO crystal scintillators," *IEEE Trans. Nucl. Sci.*, vol. 65, no. 4, pp. 1018–1024, Apr. 2018.
- [18] C. Hu *et al.*, "Neutron-induced radiation damage in BaF<sub>2</sub>, LYSO and PWO crystals," *IEEE Trans. Nucl. Sci.*, vol. 67, no. 6, pp. 1086–1092, Jun. 2020.
- [19] F. Abusalma *et al.*, "Expression of interest for evolution of the Mu2e experiment," 2018, *arXiv:1802.02599*.
- [20] P. Schotanus, P. Dorenbos, C. W. E. van Eijk, and H. J. Lamfers, "Suppression of the slow scintillation light output of BaF<sub>2</sub> crystals by La<sup>3+</sup> doping," *Nucl. Instrum. Methods Phys. Res. A, Accel. Spectrom. Detect. Assoc. Equip.*, vol. 281, no. 1, pp. 162–166, Aug. 1989.
- [21] C. L. Woody, P. W. Levy, and J. A. Kierstead, "Slow component suppression and radiation damage in doped BaF<sub>2</sub> crystals," *IEEE Trans. Nucl. Sci.*, vol. 36, no. 1, pp. 536–542, Feb. 1989.
- [22] P. A. Rodnyi, M. A. Terekhin, and E. N. Mel'chakov, "Radiative core-valence transitions in barium-based fluorides," *J. Lumin.*, vol. 47, no. 6, pp. 281–284, Mar. 1991.

- [23] B. P. Sobolev, E. A. Krivandina, S. E. Derenzo, and W. W. Moses, "Suppression of BaF<sub>2</sub> slow component of X-ray luminescence in nonstoichiometric Ba<sub>0.9</sub>R<sub>0.1</sub>F<sub>2.1</sub> crystals (R=rare earth element)," *MRS Online Proc. Library*, vol. 348, pp. 227–283, Dec. 1994.
- [24] A. I. Nepomnyashchikh, E. A. Radzhabov, A. V. Egranov, V. F. Ivashechkin, A. S. Istomin, and T. Kurobori, "Defect formation in BaF<sub>2</sub> crystals doped with cadmium," *Nucl. Instrum. Methods Phys. Res. A, Accel. Spectrom. Detect. Assoc. Equip.*, vol. 537, nos. 1–2, pp. 27–30, Jan. 2005.
- [25] E. Radzhabov, A. Istomin, A. Nepomnyashikh, A. Egranov, and V. Ivashechkin, "Exciton interaction with impurity in barium fluoride crystals," *Nucl. Instrum. Methods Phys. Res. A, Accel. Spectrom. Detect. Assoc. Equip.*, vol. 537, nos. 1–2, pp. 71–75, Jan. 2005.
- [26] A. S. Myasnikova, E. A. Radzhabov, and A. V. Egranov, "Extrinsic luminescence of BaF<sub>2</sub>:R<sup>3+</sup> crystals (R<sup>3+</sup> = La<sup>3+</sup>, Y<sup>3+</sup>, Yb<sup>3+</sup>)," *Phys. Solid State*, vol. 50, no. 9, pp. 1644–1647, Sep. 2008.
- [27] S. Diehl, R. W. Novotny, B. Wohlfahrt, and R. Beck, "Readout concepts for the suppression of the slow component of BaF<sub>2</sub> for the upgrade of the TAPS spectrometer at ELSA," *J. Phys., Conf. Ser.*, vol. 587, Feb. 2015, Art. no. 012044.
- [28] F. Yang, J. Chen, L. Zhang, C. Hu, and R.-Y. Zhu, "La and La/Ce doped BaF<sub>2</sub> crystals for future HEP experiments at the energy and intensity frontiers. Part I," *IEEE Trans. Nucl. Sci.*, vol. 66, no. 1, pp. 506–511, Jan. 2019.
- [29] F. Yang, J. Chen, L. Zhang, C. Hu, and R.-Y. Zhu, "La- and La-/Ce-doped BaF<sub>2</sub> crystals for future HEP experiments at the energy and intensity frontiers. Part II," *IEEE Trans. Nucl. Sci.*, vol. 66, no. 1, pp. 512–518, Jan. 2019.
- [30] J. Chen *et al.*, "Slow scintillation suppression in yttrium doped BaF<sub>2</sub> crystals," *IEEE Trans. Nucl. Sci.*, vol. 65, no. 8, pp. 2147–2151, Aug. 2018.
- [31] C. Hu, C. Xu, L. Zhang, Q. Zhang, and R.-Y. Zhu, "Development of yttrium-doped BaF<sub>2</sub> crystals for future HEP experiments," *IEEE Trans. Nucl. Sci.*, vol. 66, no. 7, pp. 1854–1860, Jul. 2019.
- [32] S. Gundacker *et al.*, "Vacuum ultraviolet silicon photomultipliers applied to BaF<sub>2</sub> cross-luminescence detection for high-rate ultrafast timing applications," *Phys. Med. Biol.*, vol. 66, no. 11, Jun. 2021, Art. no. 114002.
- [33] Z. Y. Wei, R. Y. Zhu, H. Newman, and Z. W. Yin, "Light yield and surface treatment of barium fluoride crystals," *Nucl. Instrum. Methods Phys. Res. B, Beam Interact. Mater. At.*, vol. 61, no. 1, pp. 61–66, Jul. 1991.
- [34] R.-Y. Zhu, "On quality requirements to the barium fluoride crystals," *Nucl. Instrum. Methods Phys. Res. A, Accel. Spectrom. Detect. Assoc. Equip.*, vol. 340, pp. 442–457, Mar. 1994.
- [35] D. Hitlin, "Progress on a photosensor for the readout of the fast scintillation light component of BaF<sub>2</sub>," presented at the CPAD Workshop, Stony Brook, NY, USA, Mar. 2021. [Online]. Available: [https://indico.fnal.gov/event/46746/contributions/210202/attachments/141121/177609/Hitlin\\_CPAD\\_210318-.pdf](https://indico.fnal.gov/event/46746/contributions/210202/attachments/141121/177609/Hitlin_CPAD_210318-.pdf)
- [36] C. Hu, L. Zhang, and R.-Y. Zhu, "Development of novel inorganic scintillators for future high energy physics experiments," presented at the CPAD Workshop, Stony Brook, NY, USA, 2021. [Online]. Available: [http://www.hep.caltech.edu/~zhu/talks/4Mu2eII\\_210303\\_BaF.pdf](http://www.hep.caltech.edu/~zhu/talks/4Mu2eII_210303_BaF.pdf)
- [37] W. Zheng, L. Jia, and F. Huang, "Vacuum-ultraviolet photon detections," *iScience*, vol. 23, no. 6, Jun. 2020, Art. no. 101145.
- [38] L. Jia, W. Zheng, and F. Huang, "Vacuum-ultraviolet photodetectors," *PhotonIX*, vol. 1, no. 1, p. 22, Nov. 2020.